

Magnetic-field control of visons in Kitaev quantum spin liquids under energy dissipation

Chihiro HARADA, Atsushi ONO, and Joji NASU

Department of Physics, Tohoku University

Sendai 980-8578

1 Introduction

Insulating magnets that remain disordered even at zero temperature due to strong quantum fluctuations are known as quantum spin liquids (QSLs). They have been the subject of extensive research since the pioneering proposal by P. W. Anderson [1]. In particular, the Kitaev model has garnered significant attention in recent years, as it provides an exactly solvable QSL ground state and offers promising applications in topological quantum computing [2].

The Kitaev model is an $S = 1/2$ quantum spin system with bond-dependent Ising-type interactions on a two-dimensional honeycomb lattice [3, 4]. Elementary excitations in this model are characterized by the fractionalization of spin degrees of freedom into two types of quasiparticles: itinerant Majorana fermions and localized excitations known as visons. When a weak magnetic field is applied, an energy gap opens in the Majorana fermion spectrum, stabilizing a chiral spin liquid. In this phase, each vison hosts a zero-energy state of a Majorana fermion, referred to as a Majorana zero mode. The composite particle formed by a vison and its associated Majorana zero mode behaves as a non-Abelian anyon, obeying exotic exchange statistics distinct from those of bosons or fermions and serving as a fundamental building block for topological quantum computation.

To utilize such non-Abelian anyons for quantum computation, it is essential not only to

observe them but also to enable their creation, manipulation, and annihilation in a well-controlled manner. While theoretical studies have proposed methods to detect the spatial positions of these anyons [5, 6], less is known for their real-time dynamics. Since the Kitaev model is a quantum spin model, the control of non-Abelian anyons might be achieved by applying external magnetic fields.

In this report, we explore the possibility of vison control by numerically simulating the time evolution of excited states in QSLs. In our previous studies, we introduced time-dependent local magnetic fields to achieve vison control and performed numerical simulations of the corresponding dynamics [7]. We also demonstrated the importance of including energy relaxation processes to stabilize such control, where energy dissipation can suppress the smearing of the vison wave function accompanied by a Majorana zero mode, thereby enabling stable manipulation of non-Abelian anyons [8]. In addition to reviewing these findings, we present a detailed analysis of the time evolution of the total energy and demonstrate that two distinct time scales emerge, attributed to spin fractionalization into two quasiparticles during the energy relaxation process.

2 Model

The Kitaev model, proposed by A. Kitaev [2], is a quantum spin model with $S = 1/2$ spins

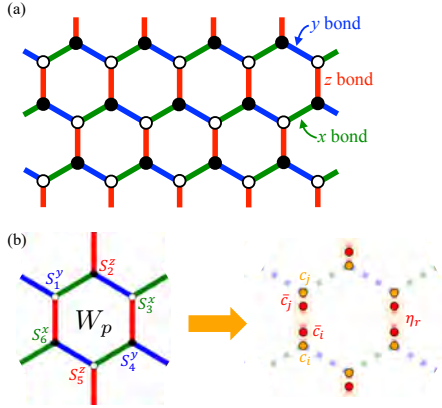


Figure 1: (a) Schematic illustration of the lattice structure on which the Kitaev model is defined. Green, blue, and red lines represent the x , y , and z bonds, respectively. Filled and open circles are sites belonging to the A and B sublattices, respectively. (b) Schematic picture of the \mathbb{Z}_2 flux operator W_p defined on the hexagonal plaquette p and its Jordan-Wigner transformation representation, where Majorana fermions c_j and \bar{c}_j , which are represented by orange and red circles, respectively, are introduced at each site. The \mathbb{Z}_2 variable η_r is defined on each z bond r .

defined on a honeycomb lattice, as shown in Fig. 1(a), and its Hamiltonian is given by

$$\begin{aligned} \mathcal{H}_K = & -J \sum_{\langle ij \rangle_x} S_i^x S_j^x - J \sum_{\langle ij \rangle_y} S_i^y S_j^y - J \sum_{\langle ij \rangle_z} S_i^z S_j^z, \end{aligned} \quad (1)$$

where J is the coupling constant for the three types of bonds, and $\langle ij \rangle_\gamma$ denotes the nearest-neighbor sites connected by the bond $\gamma = x, y, z$ [see Fig. 1(a)]. Note that the honeycomb lattice can be decomposed into two sublattices, A and B , as shown in Fig. 1(b).

To solve this model, we apply the Jordan-Wigner transformation, which maps the spin operators to Majorana fermions c_j and \bar{c}_j , as follows: $S_j^x = \frac{1}{2}c_j\tau_j$, $S_j^y = -\frac{1}{2}\bar{c}_j\tau_j$, and $S_j^z = \frac{i}{2}c_j\bar{c}_j$ for j belonging to the A sublattice, and $S_j^x = \frac{1}{2}\bar{c}_j\tau_j$, $S_j^y = -\frac{1}{2}c_j\tau_j$, and $S_j^z = \frac{i}{2}\bar{c}_j\tau_j$ for j belonging to the B sublattice, where $\tau_j =$

$\prod_{j' \neq j} (-2S_{j'}^z)$ [9–14]. This transformation is schematically illustrated in Fig. 1(c). Using this transformation, the Hamiltonian can be expressed in terms of Majorana fermions as follows:

$$\begin{aligned} \mathcal{H}_K = & -\frac{iJ_x}{4} \sum_{\langle ij \rangle_x} c_i c_j - \frac{iJ_y}{4} \sum_{\langle ij \rangle_y} c_i c_j - \frac{iJ_z}{4} \sum_{\langle ij \rangle_z} \eta_r c_i c_j, \end{aligned} \quad (2)$$

where r is the label of the z -bond, and $\eta_r = i\bar{c}_i\bar{c}_j$ is a \mathbb{Z}_2 variable taking values of ± 1 , defined on each z -bond.

In this model, there is a conserved \mathbb{Z}_2 quantity called flux W_p on each hexagonal plaquette p , defined by the product of the spin operators as

$$W_p = 2^6 \prod_{j \in p} S_j^\gamma, \quad (3)$$

where the component γ is determined as shown in Fig. 1(b). Moreover, this quantity can be expressed as $W_p = \prod_{r \in p} \eta_r$, indicating that the flux is written solely in terms of $\{\bar{c}_j\}$ and is independent of the Majorana fermions $\{c_j\}$. Since $[\mathcal{H}_K, W_p] = [\mathcal{H}_K, \eta_r] = 0$, the eigenstates of the Hamiltonian can be classified by the eigenvalues of W_p , which take values ± 1 , or equivalently by those of η_r . The ground state of the Hamiltonian belongs to the sector with $W_p = 1$ for all p , which is called the flux-free sector [2, 15]. Flux sectors with $W_p = -1$ correspond to excited states of the system, and each flux with $W_p = -1$ is regarded as a local excitation. This excitation is called a vison.

Here, we apply a uniform magnetic field to \mathcal{H}_K . Unfortunately, magnetic fields violate the exact solvability of the model since they do not commute with the flux operator W_p . To avoid this difficulty, Kitaev introduced a weak magnetic field term \mathcal{H}_κ using third-order perturbation theory [2]:

$$\mathcal{H}_\kappa = -\kappa \sum_{\langle\langle jj'j''\rangle\rangle_{\gamma\gamma'\gamma''}} S_j^\gamma S_{j'}^{\gamma'} S_{j''}^{\gamma''}, \quad (4)$$

where $\langle\langle jj'j''\rangle\rangle_{\gamma\gamma'\gamma''}$ denotes three neighboring sites connected by γ and γ'' bonds, and γ' is chosen to be distinct from both γ and γ'' . In the Majorana representation, \mathcal{H}_κ corresponds to next-nearest-neighbor hopping terms of $\{c_j\}$. This leads to nonzero Chern numbers for the itinerant Majorana fermions $\{c_j\}$, resulting in the emergence of chiral Majorana edge states and the quantization of the thermal Hall conductance in the zero-flux sector [2]. Additionally, when visons are excited, each vison is accompanied by a Majorana zero mode, which is a zero-energy state of Majorana fermions. We attempt to manipulate visons with Majorana zero modes by applying a local magnetic field to the system in addition to the uniform field \mathcal{H}_κ . To this end, we introduce a time-dependent local field term \mathcal{H}_h to the Hamiltonian as follows:

$$\mathcal{H} = \mathcal{H}_K + \mathcal{H}_\kappa + \mathcal{H}_h, \quad (5)$$

where \mathcal{H}_h is given by

$$\mathcal{H}_h = - \sum_j h_j(t) S_j^z. \quad (6)$$

3 Time-dependent mean-field theory

In the presence of the magnetic field \mathcal{H}_h , the Hamiltonian \mathcal{H} does not commute with the flux operator W_p , and visons can propagate throughout the system. This situation also indicates that the Majorana fermions $\{\bar{c}_j\}$ are no longer localized, and we must treat terms like $c_i c_j \eta_r$ as interactions between c - and \bar{c} -Majorana fermions, as seen, for example, in the last term of Eq. (2). To account for the interaction effects, we employ a time-dependent mean-field theory. In this framework, the term $i\bar{c}_i \bar{c}_j i c_i c_j$ is decoupled as $\langle i\bar{c}_i \bar{c}_j \rangle i c_i c_j + i\bar{c}_i \bar{c}_j \langle i c_i c_j \rangle - \langle i c_i \bar{c}_j \rangle i c_j \bar{c}_i - i c_i \bar{c}_j \langle i c_j \bar{c}_i \rangle + \langle i c_i \bar{c}_j \rangle i c_j \bar{c}_i + i c_i \bar{c}_j \langle i c_j \bar{c}_i \rangle + \text{const.}$ Using this decoupling, we can express the Hamiltonian in a quadratic form of Majorana

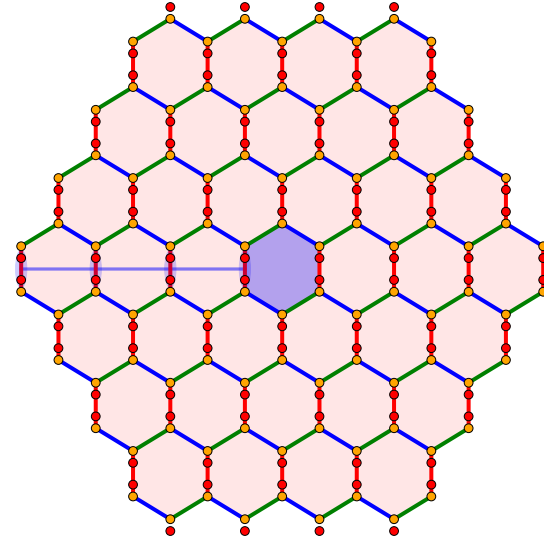


Figure 2: Schematic illustration of the vison excited on the plaquette at the center of the cluster. This vison configuration is realized by setting $\eta_r = -1$ for the z bonds intersecting with the blue line.

fermions as

$$\mathcal{H}_{\text{MF}} = \frac{i}{4} \sum_{ll'} \gamma_l \mathcal{A}_{ll'} \gamma_{l'} + C, \quad (7)$$

where $\{\gamma_l\} = \{c_1, c_2, \dots, c_N, \bar{c}_1, \dots, \bar{c}_N\}$, N is the number of sites in the system, \mathcal{A} is a $2N \times 2N$ skew symmetric matrix, and C is a constant term independent of $\{\gamma_l\}$.

To diagonalize the Hamiltonian, we adopt the Schur decomposition method for the skew-symmetric matrix \mathcal{A} . In this decomposition, the matrix \mathcal{A} is transformed into a block diagonal form by a real orthogonal matrix Q as follows:

$$Q^T \mathcal{A} Q = \begin{pmatrix} 0 & \varepsilon_1 & & & \\ -\varepsilon_1 & 0 & & & \\ & & 0 & \varepsilon_2 & \\ & & -\varepsilon_2 & 0 & \\ & & & & \ddots \\ & & & & \ddots \\ & & & & 0 & \varepsilon_N \\ & & & & -\varepsilon_N & 0 \end{pmatrix}. \quad (8)$$

In each block, the matrix $Q^T \mathcal{A} Q$ can be diagonalized, and each eigenvalue ε_λ is paired with its negative counterpart, $-\varepsilon_\lambda$.

In the present calculations, we consider the hexagon cluster shown in Fig. 2. We assume that $h_j(t) = 0$ at the initial time $t = 0$, and introduce a vison excitation in the initial state of the system. To realize this configuration, we set $\eta_r = -1$ for the z bonds intersecting with the blue line shown in Fig. 2.

We calculate the time evolution based on the mean-field Hamiltonian \mathcal{H}_{MF} . The wave function $|\Psi(t)\rangle$ obeys the Schrödinger equation, expressed as

$$i \frac{\partial}{\partial t} |\Psi(t)\rangle = \mathcal{H}_{\text{MF}}(t) |\Psi(t)\rangle. \quad (9)$$

Here, we introduce the density matrix $\rho_{ll'}(t)$, defined as

$$\rho_{ll'}(t) = \frac{1}{2} \langle \Psi(t) | \gamma_{l'} \gamma_l | \Psi(t) \rangle. \quad (10)$$

From Eq. (9), we derive the following von Neumann equation:

$$\frac{\partial \rho}{\partial t} = [\mathcal{A}, \rho]. \quad (11)$$

We evaluate the time evolution of the mean fields $\langle \Psi(t) | \gamma_{l'} \gamma_l | \Psi(t) \rangle$ using this equation. Note that, since \mathcal{A} is a sparse matrix, the commutator $[\mathcal{A}, \rho]$ can be computed efficiently even when the system size becomes large [16–18]. In this study, we employ the fourth-order Runge-Kutta method with a time step of $\Delta t/J^{-1} = 0.01$ for the time evolution.

4 Relaxation time approximation

To achieve long-range and long-time control of non-Abelian anyons in realistic setups, it is essential to suppress both the excitation of Majorana fermions and the spreading of the vison wave function. This can be achieved by allowing the energy injected by applied magnetic fields to dissipate from the system [8]. In this work, we incorporate the effect of energy dissipation into the system by considering coupling to an external environment, which is

inevitably present in any real system. Specifically, we modify the original equation given in Eq. (11) into the following form:

$$\frac{\partial \rho}{\partial t} - [\mathcal{A}, \rho] = I[\rho] \quad (12)$$

Here, the newly introduced term $I[\rho]$ represents a quantum-mechanical scattering term. We assume that the system is coupled to a thermal bath at sufficiently low temperature, and that this term drives the system toward lower energy by dissipating excess energy into the environment.

Regarding the timescale of relaxation, we assume that the relaxation to the instantaneous ground state of \mathcal{H}_{MF} , determined by the mean fields at time t , occurs much faster than the relaxation to the true ground state of the entire system, which does not contain any visons. Within this timescale, it is sufficient to consider only the former relaxation process. Under this assumption, we adopt a relaxation-time approximation for the scattering term $I[\rho]$ in Eq. (12), where the system instantaneously relaxes toward $\rho_g(t)$, the density matrix of the ground state of the instantaneous Hamiltonian $\mathcal{H}_{\text{MF}}(t)$ at time t . In the relaxation-time approximation, the scattering term is expressed as

$$\frac{\partial \rho}{\partial t} - [\mathcal{A}, \rho] = -\frac{\rho(t) - \rho_g(t)}{\tau}, \quad (13)$$

where τ is the relaxation time.

5 Results

In this section, we present the results of the time evolution from the initial state containing a vison in the system. Numerical calculations are performed in a hexagonal cluster with $N = 726$.

5.1 Effect of relaxation time

First, we discuss the effect of the relaxation time τ on the time evolution of the system. We prepare the initial state with a vison at the

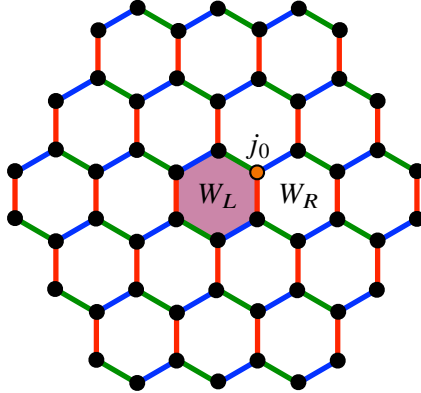


Figure 3: Schematic illustration of the initial state with a vison at the plaquette L with $W_L = -1$. The site j_0 at which the local magnetic field is applied is also presented. By applying the local field, the vison is expected to move to the right neighboring plaquette R .

center of the cluster and apply a local magnetic field at the upper right site j_0 of the plaquette with $W_p = -1$, as presented in Fig. 3. By applying the local magnetic field, the vison is expected to move to the right neighboring plaquette $p' = R$. We also refer to the plaquette p where the vison is initially located as $p = L$. The time dependent local magnetic field at site j_0 is chosen as $h_{j_0}(t) = A\theta(t)\theta(t_{\max} - t)$, where $\theta(t)$ is the Heaviside step function and t_{\max} is the time when the magnetic field is turned off. In this situation, $\langle W_L \rangle + \langle W_R \rangle = 0$ is satisfied, and the local field is turned off when $\langle W_L \rangle = \langle W_R \rangle = 0$. Note that the flux operators W_L and W_R are conserved quantities when $h_{j_0} = 0$, and their expectation values are time-dependent only when $A \neq 0$. Based on the previous study [19], we set the relaxation time τ to be in the range of $10 \lesssim \tau/J^{-1} \lesssim 50$. We also introduce $D_p = (1 - \langle W_p \rangle)/2$, which corresponds to the vison density at plaquette p .

Figure 4(a) shows the time evolution of the vison density with $\kappa/J = 0.1$ and $\tau/J^{-1} = 20$,

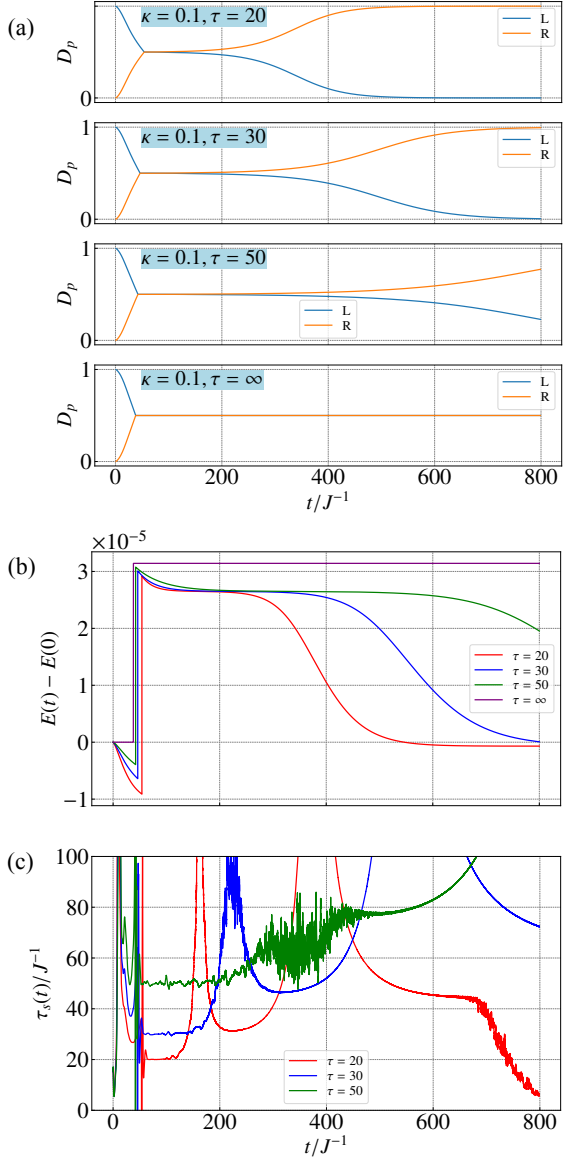


Figure 4: Time evolution of (a) the vison density at the plaquette L and R (see Fig. 3), (b) the total energy $E(t)$, and the relaxation time $\tau_s(t)$, by applying a local magnetic field with $A/J = 0.08$ at the site j_0 in the system with $N = 726$ and $\kappa/J = 0.10$ in the presence of energy dissipation with the several relaxation times.

30 , 50 , and ∞ in the presence of a time-dependent local magnetic field with $A/J = 0.08$. In the case of $\tau = \infty$, which corresponds to the situation without relaxation, the vison density does not change after t_{\max} . This result suggests that the vison is delocalized over both

the L and R plaquettes when relaxation is not taken into account. On the other hand, for finite values of τ , the vison density D_p tends to become localized at the right plaquette R after the magnetic field is turned off. The relaxation proceeds more rapidly for smaller values of τ . Note that the vison density D_p at plaquette R approaches 1 in the presence of relaxation. Based on these results, one can interpret that, in the presence of energy relaxation, spatially extended visons are energetically unstable, which is consistent with a previous study [20], and that an excited vison gradually shrinks into one of the plaquettes as the system relaxes.

To investigate the time evolution of the system in more detail, we also analyze the total energy $E(t)$, which is defined as $E(t) = \langle \Psi(t) | \mathcal{H} | \Psi(t) \rangle / N$. Figure 4(b) shows $E(t) - E(0)$ as a function of t for $\tau = 20, 30, 50$, and ∞ . In the case without relaxation ($\tau = \infty$), the total energy is conserved when the magnetic field remains unchanged. In the presence of relaxation, the total energy decreases before the local magnetic field is turned off. The energy reduction is more pronounced for smaller τ . At $t = t_{\max}$, the total energy abruptly increases due to the loss of energy gain from the Zeeman term \mathcal{H}_h , similarly to the case without relaxation. In the presence of relaxation, the total energy gradually decreases after the abrupt increase. We find that the energy relaxation proceeds in two distinct stages.

Immediately after the magnetic field is turned off, energy relaxation begins. During this period, as shown in Fig. 4(a), the vison densities D_p for $p = L, R$ remain nearly constant, suggesting that energy dissipation originates primarily from the itinerant Majorana fermion systems. Subsequently, a further decrease in the total energy is observed. According to Fig. 4(a), this energy reduction is accompanied by the localization of the vison at position R . At this stage, the energy approaches its initial value.

To quantitatively discuss the relaxation process, we introduce the relaxation time $\tau_s(t)$ estimated from $E(t)$, which is defined as

$$\frac{1}{\tau_s(t)} = \left| \frac{d}{dt} \ln \left(\frac{dE(t)}{dt} \right) \right| = \left| \frac{1}{dE(t)/dt} \frac{d^2 E}{dt^2} \right|. \quad (14)$$

Figure 4(c) shows the time evolution of $\tau_s(t)$ for $\tau = 20, 30$, and 50 . In the initial stage of the energy relaxation, $\tau_s(t)$ remains almost constant and is approximately equal to τ , suggesting that the energy relaxation of the itinerant Majorana fermion system is governed by the relaxation time τ . In the subsequent stage of the energy relaxation, $\tau_s(t)$ exceeds τ , indicating that the energy relaxation of the vison system proceeds more slowly than the relaxation time τ . Therefore, we conclude that the energy relaxation of Majorana fermions is clearly distinct from that of visons, and that the relaxation process can be divided into two stages, corresponding to different quasiparticles.

5.2 Comparison with the energy-conserving system

In the previous section, we showed that energy relaxation can localize the vison by applying an atomic-scale local magnetic field. To demonstrate vison manipulation in more realistic situations, we consider the case in which a local magnetic field is applied over wider regions. We perform numerical simulations in a system with $N = 726$ and $\kappa/J = 0.05$, and prepare the initial state with a vison, as shown in Figs. 5(a) and 5(b). The time evolution of the system is computed in the presence of a time-dependent local magnetic field applied to the sites indicated by yellow circles in these figures. The time dependence of the local magnetic field is modeled as a Gaussian function, which is shown on the right side of Fig. 5. In this figure, we present the time evolution of the system in the absence of relaxation (left side) and in the presence of relaxation (right side).

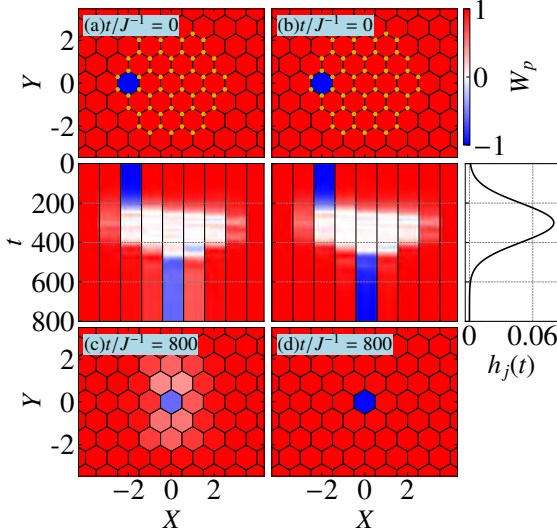


Figure 5: Comparison of the time evolution of vison driving by applying a time-dependent magnetic field in the system including $N = 726$ with $\kappa/J = 0.05$ in the absence and presence of energy dissipation. The time-dependent local field is applied to the sites indicated by yellow circles in (a) and (b). The time dependence of the local magnetic field $h_j(t)$ is shown on the right side. (a),(c) Initial and final states of the vison distribution without energy dissipation, and (b),(d) those with energy dissipation ($\tau = 50$).

Figures 5(a) and 5(c) show vison distributions of the initial and final states in the absence of relaxation. The figures between them show the time evolution of $\langle W_p \rangle$ for the plaquettes p that are crossed by the line $Y = 0$. When the amplitude of the local magnetic field reaches its maximum value, the vison is extended over the region where the local magnetic field is applied. After the local field approaches zero, the vison moves to the right side and becomes localized. As presented in Fig. 5(c), the vison is not well localized and its distribution is slightly extended. This is due to the energy injection by the local magnetic field, which is not compensated by energy relaxation.

On the other hand, in the case with relaxation, the vison is displaced by the application of the time-dependent local field and becomes well localized in the final state, as shown in Fig. 5(d), which is in stark contrast to the case without relaxation. This localized behavior is due to energy dissipation by the relaxation term, suggesting that energy relaxation is essential for the manipulation of visons.

6 Conclusion

In summary, we have investigated the time evolution of vison excitations driven by a time-dependent local magnetic field in the Kitaev model with energy dissipation. We performed numerical simulations of the time evolution for an excited vison using time-dependent mean-field theory and the relaxation time approximation. Our results show that the energy relaxation process can be divided into two distinct stages, corresponding to the relaxation of Majorana fermions and visons, respectively. Furthermore, we demonstrated that energy relaxation is essential for vison manipulation, and that visons can be localized by applying a time-dependent local magnetic field when energy dissipation is taken into account.

Acknowledgments

This work was supported by Grant-in-Aid for Scientific Research from JSPS, KAKENHI Grant Nos. JP19K03742, JP20H00122, JP20K14394, JP22H01175, JP23H01129, JP23H04859, JP23H04865, JP23K13052, JP23K25805, and No. JP24K00563. It is also supported by JST PRESTO Grant No. JPMJPR19L5. Parts of the numerical calculations were performed in the supercomputing systems in ISSP, the University of Tokyo.

References

- [1] P. W. Anderson, “Resonating valence bonds: a new kind of insulator?”, Mater. Res. Bull. **8**, 153 (1973).
- [2] A. Kitaev, “Anyons in an exactly solved model and beyond”, Ann. Phys. (N. Y.) **321**, 2 (2006).
- [3] Y. Motome and J. Nasu, “Hunting Majorana Fermions in Kitaev Magnets”, J. Phys. Soc. Jpn. **89**, 012002 (2020).
- [4] J. Nasu, “Majorana quasiparticles emergent in Kitaev spin liquid”, Prog. Theor. Exp. Phys. **2023**, ptad115 (2023).
- [5] M. Udagawa, S. Takayoshi, and T. Oka, “Scanning Tunneling Microscopy as a Single Majorana Detector of Kitaev’s Chiral Spin Liquid”, Phys. Rev. Lett. **126**, 127201 (2021).
- [6] M. O. Takahashi, M. G. Yamada, M. Udagawa, T. Mizushima, and S. Fujimoto, “Nonlocal Spin Correlation as a Signature of Ising Anyons Trapped in Vacancies of the Kitaev Spin Liquid”, Phys. Rev. Lett. **131**, 236701 (2023).
- [7] C. Harada, A. Ono, and J. Nasu, “Field-driven spatiotemporal manipulation of Majorana zero modes in a Kitaev spin liquid”, Phys. Rev. B **108**, L241118 (2023).
- [8] C. Harada, A. Ono, and J. Nasu, “Real-time control of non-abelian anyons in kitaev spin liquid under energy dissipation”, Phys. Rev. B **110**, 214426 (2024).
- [9] H.-D. Chen and J. Hu, “Exact mapping between classical and topological orders in two-dimensional spin systems”, Phys. Rev. B **76**, 193101 (2007).
- [10] X.-Y. Feng, G.-M. Zhang, and T. Xiang, “Topological Characterization of Quantum Phase Transitions in a Spin-1/2 Model”, Phys. Rev. Lett. **98**, 087204 (2007).
- [11] H.-D. Chen and Z. Nussinov, “Exact results of the Kitaev model on a hexagonal lattice: spin states, string and brane correlators, and anyonic excitations”, J. Phys. A **41**, 075001 (2008).
- [12] J. Nasu, M. Udagawa, and Y. Motome, “Vaporization of Kitaev Spin Liquids”, Phys. Rev. Lett. **113**, 197205 (2014).
- [13] J. Nasu, M. Udagawa, and Y. Motome, “Thermal fractionalization of quantum spins in a Kitaev model: Temperature-linear specific heat and coherent transport of Majorana fermions”, Phys. Rev. B **92**, 115122 (2015).
- [14] T. Minakawa, Y. Murakami, A. Koga, and J. Nasu, “Majorana-Mediated Spin Transport in Kitaev Quantum Spin Liquids”, Phys. Rev. Lett. **125**, 047204 (2020).
- [15] E. H. Lieb, “Flux phase of the half-filled band”, Phys. Rev. Lett. **73**, 2158 (1994).
- [16] N. Tsuji and H. Aoki, “Theory of Anderson pseudospin resonance with Higgs mode in superconductors”, Phys. Rev. B **92**, 064508 (2015).
- [17] Y. Murakami, D. Golež, T. Kaneko, A. Koga, A. J. Millis, and P. Werner, “Collective modes in excitonic insulators: Effects of electron-phonon coupling and signatures in the optical response”, Phys. Rev. B **101**, 195118 (2020).
- [18] J. Nasu, Y. Murakami, and A. Koga, “Scattering phenomena for spin transport in a Kitaev spin liquid”, Phys. Rev. B **106**, 024411 (2022).
- [19] M. Kanega, T. N. Ikeda, and M. Sato, “Linear and nonlinear optical responses in Kitaev spin liquids”, Phys. Rev. Res. **3**, L032024 (2021).
- [20] V. Lahtinen, “Interacting non-Abelian anyons as Majorana fermions in the honeycomb lattice model”, New J. Phys. **13**, 075009 (2011).